AGU PUBLICATIONS

Geophysical Research Letters

RESEARCH LETTER
10.1002/2016GL071298

The scaling exponent of residual nonwetting phase cluster size distributions in porous media

Stefan Iglauer[1] **and Wolfgang Wülling**[1]

[1]Department of Petroleum Engineering, Curtin University, Kensington, Western Australia, Australia

Key Points:
- The residual cluster size distribution exponent tau is substantially smaller (1.1) than previously suggested
- Hydrocarbon recovery is easier than predicted, but CO_2 geostorage dissolution trapping capacities are significantly reduced
- This raises increasing doubt that percolation models can accurately predict subsurface fluid flow behavior

Correspondence to:
S. Iglauer,
stefan.iglauer@curtin.edu.au

Citation:
Iglauer, S., and W. Wülling (2016), The scaling exponent of residual nonwetting phase cluster size distributions in porous media, *Geophys. Res. Lett.*, *43*, 11,253–11,260, doi:10.1002/2016GL071298.

Received 19 JUL 2016
Accepted 8 OCT 2016
Accepted article online 11 OCT 2016
Published online 5 NOV 2016

Abstract During an imbibition process in two-phase subsurface flow the imbibing phase can displace the nonwetting phase up to an endpoint at which a residual saturation is reached (which cannot be reduced further by additional wetting phase flow due to the complex pore network of the rock and associated strong capillary forces which trap the nonwetting phase). The residual nonwetting phase is split into many disconnected clusters of different sizes. This size distribution is of key importance, for instance, in the context of hydrocarbon recovery, contaminant transport, or CO_2 geostorage; and it is well established that this size distribution follows a power law. However, there is significant uncertainty associated with the exact value of the distribution exponent τ, which mathematically describes the size distribution. To reduce this uncertainty and to better constrain τ, we analyzed a representative experimental data set with mathematically rigorous methods, and we demonstrate that τ is substantially smaller ($\approx$1.1) than previously suggested. This raises increasing doubt that simple percolation models can accurately predict subsurface fluid flow behavior; and this has serious consequences for subsurface flow processes: hydrocarbon recovery is easier than predicted, but CO_2 geostorage dissolution trapping capacities are significantly reduced and potential remobilization of residual CO_2 is more likely than previously believed.

1. Introduction

A phenomenon of key importance in multiphase flow through geological porous media is the formation of a residual phase when one phase is displaced by another immiscible (or partially miscible) phase. The characteristics of such a residual phase determine CO_2 geostorage capacities (*residual trapping* [*Suekane et al.*, 2008; *Pentland et al.*, 2011; *Iglauer et al.*, 2011]), oil and gas recovery efficiency (this is the volume of hydrocarbon which cannot be produced by conventional means [*Lake*, 2010; *Iglauer et al.*, 2010, 2013]), and contaminant transport and clean-up of nonaqueous liquids from soil (e.g., spilled organic solvents or crude oil) [*Sleep and McClure*, 2001]. Apart from saturation, the most important property of the residual phase is its cluster (droplet) size distribution inside the pore network of the rock.

Many researchers have measured this cluster size distribution, initially by solidifying injected styrene monomers and dissolving rock [*Chatzis et al.*, 1983], and nowadays by X-ray microcomputed tomography imaging [*Iglauer et al.*, 2010, 2011, 2012, 2013, 2014; *Chaudhary et al.*, 2013; *Georgiadis et al.*, 2013; *Geistlinger and Mohammadian*, 2015; *Andrew et al.*, 2014; *Prodanovic et al.*, 2007; *Kumar et al.*, 2009, 2012; *Karpyn et al.*, 2010]. Most of the researchers reported that the cluster size distribution follows a power law $N(s) \sim s^{-\tau}$, where $N(s)$ is the count number of a cluster of size s and τ is the scaling exponent (reported values for τ ranged between 1.8 and 2.3). This scaling exponent is physically of high significance: A smaller τ implies overall larger residual droplets, which are easier to mobilize [*Herring et al.*, 2013; *Wardlaw and Li*, 1988] and thus lead to higher oil recoveries in the context of hydrocarbon production or solvent recovery from contaminated soil, particularly when chemically enhanced methods are used [e.g., *Iglauer et al.*, 2010]. However, larger drops also pose a higher risk for CO_2 geostorage schemes as CO_2 remobilization of residual CO_2 is more likely in case of larger drops. Moreover, larger drops also have a smaller surface-to-volume ratio, which leads to smaller CO_2-dissolution trapping capacities [*Riaz et al.*, 2006; *Pentland et al.*, 2012] and less mass transfer between the solvent phase and the aqueous phase in case of soil contamination. However, the τ values in the literature have a large uncertainty mainly due to the methods used to extract τ.

We will show here—by using a mathematically rigorous statistical analysis—that τ is substantially lower than previously concluded ($\approx$1.1). This raises increasing doubt that simple percolation models can accurately

10.1002/2016GL071298

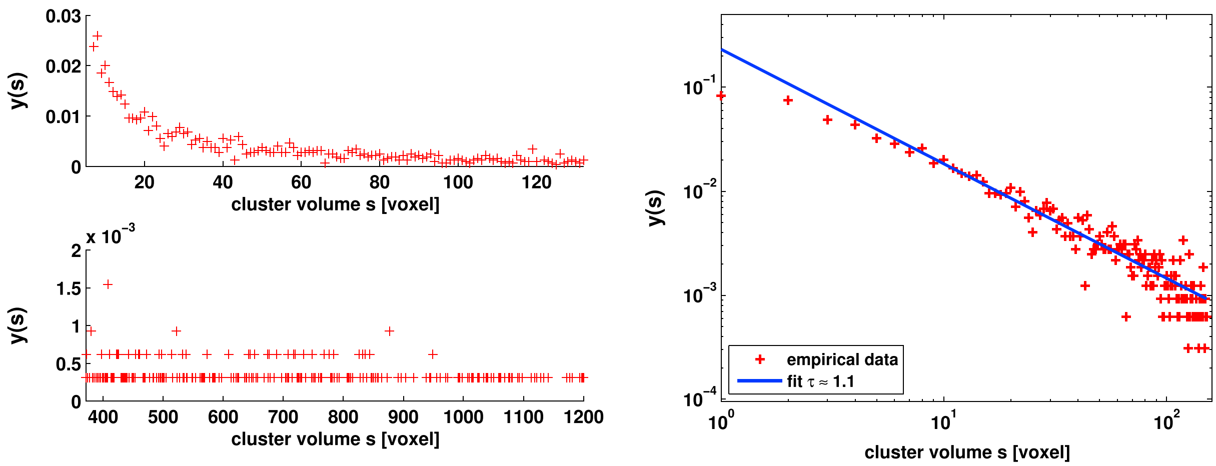

Figure 1. Plot of empirical frequencies. (top left) The graph shows the range when the droplet number rapidly decreases; (bottom left) the graph displays scarcity of tail observations for $s > 400$. The volume unit is voxel, 1 voxel = $(3.5\mu m)^3$. (right) The graph shows a logarithmic plot of the empirical frequencies. The data reveal an approximately linear relation for smaller volumes s—we also see the expected increasing scatter for larger volumes.

predict subsurface flow behavior. Furthermore, as mentioned above, a smaller τ has serious implications: hydrocarbon recovery is more efficient than predicted, but CO_2 geostorage is more risky.

2. Cluster Size Distribution

We examine a typical residual cluster size distribution data set, which we recently measured. The data were acquired through an X-ray microcomputed tomography experiment: a small (water-wet) sandstone rock volume at residual oil saturation $(3\ mm)^3$ was imaged at high resolution $(3.5\ \mu m)^3$, and the raw image was filtered with a nonlocal means filter [*Buades et al.*, 2005] and segmented with a watershed algorithm [*Schlüter et al.*, 2014]. Specifically, homogeneous and clean Bentheimer sandstone (porosity 23.0%; brine permeability 1700 mD; medium grain size 180 μm; pore size range from 1 to 340 μm [*Al-Yaseri et al.*, 2015; *Maloney et al.*, 1990]) was completely filled with brine, and oil (n-decane) was injected at a high capillary number (3×10^{-4}) so that an initial oil saturation of 68.5% was achieved. This mimics an oil reservoir. Subsequently, we flooded the sandstone plug with brine at a low capillary number of 7×10^{-7} (which is representative of subsurface conditions), until no more oil was produced and the residual oil saturation state was achieved. The detailed experimental procedure is described elsewhere [*Iglauer et al.*, 2010, 2012, 2014]. Our experimental data are as follows: We observed $n = 3240$ individual (disconnected) oil clusters, among which $\tilde{n} = 525$ different cluster volumes occurred, (the cluster volume s is given in voxels, note that here 1 voxel = $(3.5\ \mu m)^3$ = 24.875 μm^3). That means that among the 3240 individually observed clusters there were, for instance, 60 clusters with a volume $s = 9$ voxels, so $N(9) = 60$. The normalized frequencies are

$$y(s) = N(s)/n,$$

and they can be interpreted as an empirical analogue to precise but unknown probabilities as defined in equation (1). By visual inspection of the data (Figure 1, left column) it is clear that the number $N(s)$ of clusters of volume s drops rapidly, and it is thus plausible to assume a power law relation. Another way to visually check the possibility of a power law relation is to generate a logarithmic plot of these frequencies or volume counts, respectively, and if such a graph reveals approximately a linear relation, a power law is assumed, see Figure 1 (right). The power law relation is usually expressed as $N(s) \sim s^{-\tau}$, see above. One key task is to derive the exponent τ. In the next sections we will thus estimate τ with rigorous and nonrigorous statistical techniques.

3. Statistical Analysis

When dealing with a power law the quantity of interest, N, is usually written as $N \sim s^{-\tau}$, i.e., a power law multiplied with a scalar. What is more, the range on which the power law holds is specified by its lower bound $s_{\min}$ and the right upper bound $s_{\max} > s_{\min}$; i.e.,

$$f(s) = \begin{cases} \alpha s^{-\tau} & , \ s_{\min} \leq s \leq s_{\max} \\ 0 & , \ \text{otherwise.} \end{cases} \tag{1}$$

If the data one is working with are continuous, i.e., $s \in \mathbb{R}_+$, then $f(s)$ in (1) represents a density function and the normalizing constant thus becomes $\alpha = \left[\int_{s_{\min}}^{s_{\max}} x^{-\tau}\,\mathrm{d}x\right]^{-1}$. As the residual clusters have specific volumes (number of voxels), they are discrete, $s \in \mathbb{N}$, and in case of a discrete model, the function $f(s)$ in (1) represents the probabilities and the normalizing constant α is thus $\alpha = \left[\sum_{r=s_{\min}}^{s_{\max}} r^{-\tau}\right]^{-1}$. Now with $\zeta(\tau)$ being the (famous), Riemann zeta-function and defining the generalized zeta-function [see, e.g., *Clauset et al.*, 2009] as $\zeta(\tau, s) = \zeta(\tau) - \sum_{r=1}^{s-1} r^{-\tau}$ the normalizing constant of a discrete power law can be written as

$$\alpha = \left[\sum_{r=s_{\min}}^{s_{\max}} r^{-\tau}\right]^{-1} = \left[\zeta(\tau, s_{\min}) - \zeta(\tau, s_{\max}+1)\right]^{-1}.$$

This last equation allows a convenient calculation of α by mathematical software packages (those which have implemented an evaluation routine of the Riemann zeta-function) when $s_{\max}$ is particularly large, or when $s_{\max} = \infty$. Further, we denote the cumulative distribution function (CDF) of a power law as $F(s)$.

Since our data are discrete, $s \in \mathbb{N}$, it is natural to work with the discrete model. However, the data we have are voxelated, which means they are the result of rounding real numbers to integer numbers, and for this reason one might suspect that we have to choose the continuous model, because in theory the cluster volumes can take on theoretically any value in $\mathbb{R}_+$, whereas the fact that our data are discrete is only due to a specific measurement method. Therefore, let $\tilde{N}$ be a positive, continuous random variable, i.e., $\tilde{N} \in \mathbb{R}_+$, which follows a continuous power law. Next we define a second random variable N which is derived by rounding the values of $\tilde{N}$ to the nearest integer number,

$$N = \mathrm{round}(\tilde{N}) \in \mathbb{N}.$$

Making use of a standard Taylor expansion of $F(s \pm 0.5)$, it is straightforward to approximate the probabilities of N as follows:

$$\begin{aligned}
\mathrm{Prob}(N = s) &= \mathrm{Prob}(\tilde{N} \in (s - 0.5, s + 0.5]) \\
&= F(s + 0.5) - F(s - 0.5) \\
&= f(s) \underbrace{\left(1 + \frac{\tau(1+\tau)}{24s^2} + \mathcal{O}\left(\frac{1}{s^4}\right)\right)}_{\text{factor}}.
\end{aligned}$$

Now if, e.g., $\tau = 1.1$ and $s \geq 10$, we obtain $1 \leq \text{factor} \leq 1.001$, which means that N, too, follows (approximately) a power law having the same scaling exponent τ: $N \sim s^{-\tau}$. We therefore limit our discussion to discrete power laws.

3.1. Summation Methods

Two methods for estimating the scaling exponent τ have been proposed and have frequently been used in the literature [see *Dias and Wilkinson*, 1986]. We have called them summation methods, because they involve sums of empirical data as approximations of cumulative functions; both methods are in essence linear regressions. The first one is based on an approximation of the cumulative probability $P(s) = \mathrm{Prob}(N \geq s)$, i.e.,

$$P(s) = \int_s^{\infty} \mathrm{d}F(t) = \sum_{r=s}^{\infty} f(r), \tag{2}$$

where the second identity holds since we are considering a discrete power law. Instead of considering the empirical analogue $P_{\mathrm{emp}}(s) = \sum_{r \geq s} y(r)$, it is argued in *Dias and Wilkinson* [1986, (3.6)] that taking the sum

$$\tilde{P}(s) = \sum_{r=s}^{2s-1} y(r)$$

would be a natural way to approximate $P(s)$. For this reason $\tilde{P}(s)$ should scale as $s^{1-\tau}$ for $1 \ll s \ll s_{\max}$ [*Dias and Wilkinson*, 1986, (3.6) and (3.7)]. The exponent τ is then derived by fitting a straight line through a logarithmic plot of $\tilde{P}(s)$. However, since the frequencies $y(r)$ are summed up to just $2s - 1$ we always have $\tilde{P}(s) < P_{\mathrm{emp}}(s)$; hence, this method has a tendency to systematically overestimate τ. In addition, the range in which the straight-line fit is applied depends on the researcher's discretion. For instance, with the typical data we are examining here, applying the fit based on $\tilde{P}(s)$ in the range of $s = 38, \dots, 71$ leads to $\hat{\tau} \approx 1.28$, whereas if we choose the range $s = 38, \dots, 81$ we obtain $\hat{\tau} \approx 1.44$.

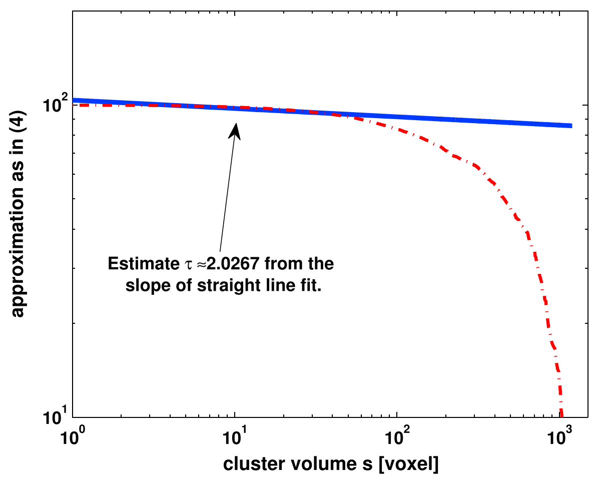

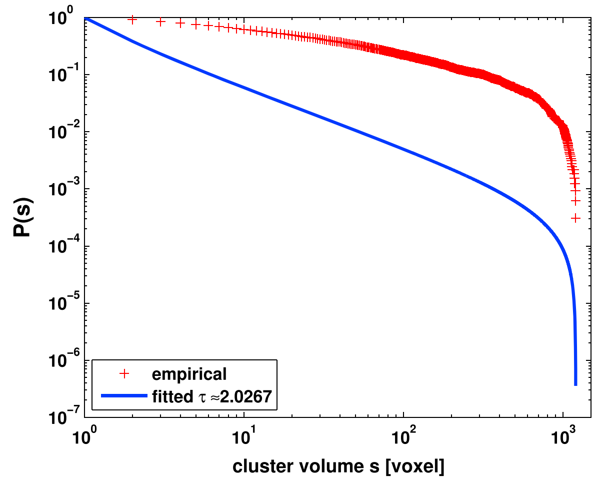

Figure 2. (left) The typical plot when the scaling exponent τ is being extracted from a straight-line fit through a logarithmic plot of $\tilde{M}(s)$, which is displayed as the red dashed dotted line. We have applied a straight-line fit in the range of volumes up to $s = 50$. Using the method from *Dias and Wilkinson* [1986, (3.8) and (3.9)], the derived scaling exponent is $\hat{\tau} = 2$—slope of the straight-line fit ≈ 2.0267. (right) Logarithmic plots of cumulative functions in the full range of $[1, 1200]$. The blue solid line displays (2) for the derived τ value of $\hat{\tau} \approx 2.0267$, and the red cross signs are the empirical equivalent to $P(s)$, i.e., $P_{\mathrm{emp}}(s) = \sum_{r \geq s} y(r)$. One can see that these two functions do not match at all.

It is even more important to point out the bias (see Example 2 below) of the second method proposed in *Dias and Wilkinson* [1986] as it has been a standard approach in the literature. It works similarly, but this time the function to be approximated is

$$M(s) = \mathbb{E}[N, N \geq s] = \int_s^\infty t \,\mathrm{d}F(t) = \sum_{r=s}^{\infty} r f(r), \tag{3}$$

where the last identity holds for a discrete power law ($\mathbb{E}[\,]$ denotes the expectation of a random variable). In *Dias and Wilkinson* [1986] a power law with unbounded domain ($s_{\max} = \infty$) is considered; in such a case (3) exists if $\tau > 2$ and it can then be shown that $M(s)$ scales as $s^{-\tau+2}$, i.e., $M \sim s^{-\tau+2}$. Either for a power law with bounded or unbounded domain, the idea developed in *Dias and Wilkinson* [1986] is to take

$$\tilde{M}(s) = \sum_{r \geq s} r y(r) \tag{4}$$

as an approximation of $M(s)$. Then $\tilde{M}(s)$ should also scale as $s^{-\tau+2}$ [see *Dias and Wilkinson*, 1986, (3.8) and (3.9)]. However, this approach contains the assumption that the scaling exponent is known to be larger than 2, because as one can see both functions $M(s)$ and $\tilde{M}(s)$ are monotonously decreasing, whereas clearly $s^{-\tau+2}$ can only be a decreasing function for $\tau > 2$. Therefore, this method is a priori disconnected from empirical data; it is merely a way of defining τ to be larger than 2, rather than estimating it from actual observations. Applying this method to our experimental data Figure 2 shows (a) the typical graph of applying a linear regression to $\tilde{M}(s)$; carrying out this regression in the range of $s = 1, \dots, 50$, we obtain an estimated scaling parameter of $\hat{\tau} = 2.0267$; and (b) the cumulative distribution functions reveal that the fit does not match experimental data.

We illustrate this strong bias further through two examples. In the first example we analyze synthetical data; hence, we know the exact scaling exponent, and in the second example we review historical data sets from *Iglauer et al.* [2010].

Example 1. *Consider a discrete power law as in (1) in the range of $s_{\min} = 8$ and $s_{\max} = 1200$. We have sampled 3200 data from power laws with various scaling exponents τ and produced an estimate of τ via the method based on (4) with a range of $s = 8, \dots, 40$ for the straight-line fit, see Table 1.*

Table 1. Results of Example 1[a]

Original τ	Range of Straight-Line Fit	Estimated $\hat{\tau}$	Relative Error
3.0	[8, 40]	3.08	2.6%
2.5	[8, 40]	2.55	2.1%
1.9	[8, 40]	2.18	15.0%
1.5	[8, 40]	2.07	38.0%
1.1	[8, 40]	2.02	84.1%

[a]We have estimated $\hat{\tau}$ via the method based on (4). The results reveal the method's bias for $\tau > 2$.

Example 2. *Two sandstones (Clashach and Doddington) have been investigated in Iglauer et al.* [2010]*, and a scaling exponent of* $\hat{\tau} \approx 2.053$ *was derived for both samples via the estimation based on (4). Plotting the cumulative probabilities, it is obvious that the result is strongly biased, see Figure* 3.

We thus conclude that obtaining an estimation $\hat{\tau}$ of the scaling parameter through assuming that $\tilde{M}(s)$ scales as $s^{-\tau+2}$ is strongly biased. Finally, since both methods from *Dias and Wilkinson* [1986] are linear regressions, we also mention the discussion of regression pitfalls in *Clauset et al.* [2009, Appendix A].

3.2. Maximum Likelihood Estimation

The maximum likelihood method does not have such biases; instead, the maximum likelihood estimator (m.l.e.) of τ is consistent, and in addition, if an efficient estimator of τ exists, the method of maximum likelihood will generate it [*Lindgren*, 1993, chapter 8.6]. In a nutshell, the maximum likelihood method consists of determining that parameter τ, which maximizes the log–likelihood $\mathcal{L}(\tau)$ of the occurrence of experimental observations [see, e.g., *Lindgren*, 1993, chapter 8.4]. Let m be the number of observations in the range $[s_{\min}, s_{\max}]$ and let i_m be the smallest index such that $s_{i_m} = s_{\min}$. Then the log-likelihood function for a power law (1) is

$$\mathcal{L}(\tau) = -m \ln \left(\zeta(\tau, s_{\min}) - \zeta(\tau, s_{\max} + 1) \right) - \tau \sum_{j=i_m}^{m+i_m-1} \ln(s_j). \quad (5)$$

Hence, the m.l.e. $\hat{\tau}$ of τ is that number which maximizes $\mathcal{L}(\tau)$, and it can be determined by numerically maximizing (5). Note that there are two additional parameters $s_{\min}$ and $s_{\max}$ specifying the range in which the data might follow a power law. As we have seen in Figure 1, the tail observations are very scarce due to

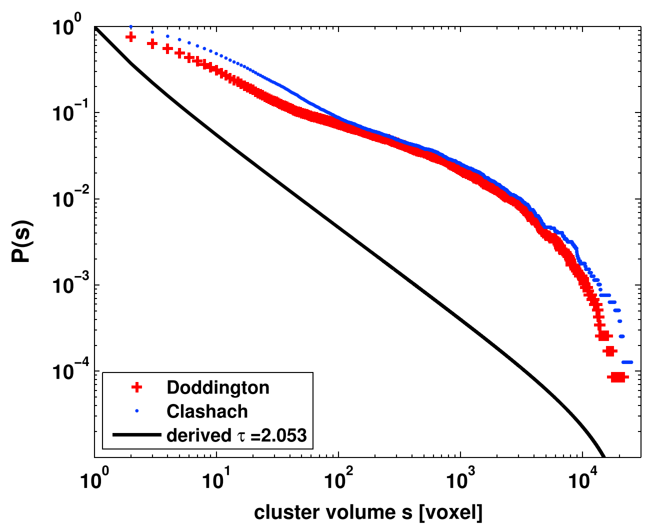

Figure 3. Logarithmic plot of cumulative probability function $P(s)$ and its empirical analogue function for data sets from *Iglauer et al.* [2010]. The black solid line represents a power law with scaling parameter $\tau = 2.053$, and as one can see it does not match with the experimental data. Also, one can see that for both empirical data sets there is a bent in the curves at approximately $s = 100$ voxels. A reason for this may be a pore throat spatial correlation at a length scale corresponding to this volume [cp. *Yang et al.*, 2015, Figures 7 and 8].

Table 2. For Various Values of s_{max} We Have Estimated $\hat{\tau}$ Assuming a Discrete Power Law With Cutoff (1) Via Maximizing (5) and Derived a Corresponding Estimate $\hat{s}_{min}$ of the Lower Bound Via Minimizing the KS Statistic (6)[a]

$\hat{s}_{min}$	s_{max}	m	$\hat{\tau}$	*p* Value
54	1200	1041	1.3811	9.9%
8	298	1871	1.1953	0.0%
8	150	1609	1.1231	10.1%
8	140	1580	1.1207	12.3%
8	130	1558	1.1040	56.6%
8	125	1538	1.1064	43.6%
8	120	1528	1.0926	94.4%

[a]In the final column we report the Monte Carlo-like *p* value, which has been developed in *Clauset et al.* [2009, section 4]; we have computed the ratio *p* as in (7) via 1000 simulations each.

experimental limitations (the observed space is finite). For this reason one might overestimate the true τ (because a larger scaling exponent implies less data in the tail). Thus, the parameters s_{min} and s_{max} have to be estimated separately.

For a power law defined on $[s_{min}, \infty)$ a method developed in *Clauset et al.* [2009] in order to estimate the lower bound s_{min} is to take that $\hat{s}_{min}$ value, which minimizes the Kolmogorov-Smirnov (KS) statistic [see, e.g., *Lindgren*, 1993, p. 480]

$$D_m = \sup_{s_{min} \le s \le s_{max}} |\hat{F}_m(s) - F_{\hat{\tau}}(s)|, \tag{6}$$

where $\hat{F}_m(s)$ denotes the empirical distribution function (for data $s \ge s_{min}$) and $F_{\hat{\tau}}(s)$ is the CDF corresponding to the estimated $\hat{\tau}$. It has been shown in *Clauset et al.* [2009] that this method of estimating $\hat{s}_{min}$ works well. As we also have to cope with a higher cutoff point we proceed as follows: We set the upper cutoff point s_{max} and then estimate $\hat{s}_{min}$ and the corresponding scaling exponent $\hat{\tau}$ through numerically maximizing (5), Table 2.

What is more, a specific goodness of fit measure has been developed in *Clauset et al.* [2009] as well. For the obtained fit the KS statistic D_m is computed. Subsequently, synthetic data consisting of two subsets are generated: One subset contains data sampled from the original empirical data in $s < \hat{s}_{min}$, and the second subset is sampled from the fitted distribution $F_{\hat{\tau}}(t)$. For this synthetically generated data another power law fit is

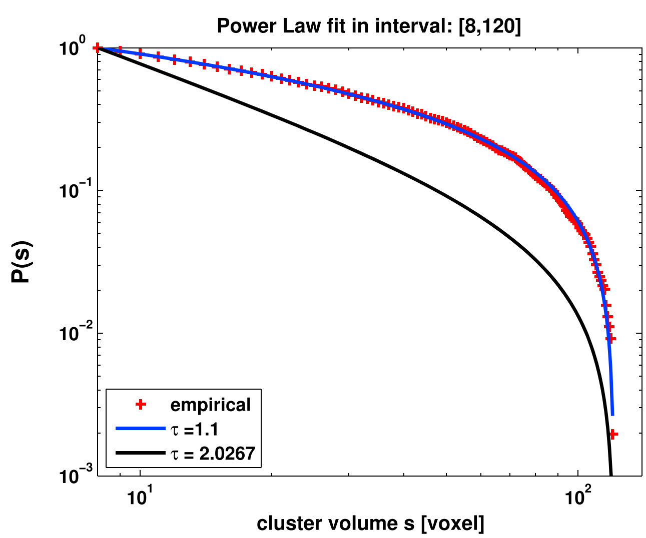

Figure 4. Power law fit with resulting scaling exponent $\hat{\tau} \approx 1.1$ versus empirical data and the fit obtained via (4), which gave $\hat{\tau} \approx 2.0267$.

applied and its KS statistic D_{synth} is then compared to D_m, i.e., the KS statistic for the original data. This procedure is repeated, here 1000 times, and we then calculate the fraction of times for which D_m is smaller or equal to D_{synth}; i.e.,

$$p = \{\text{number of times when } D_m \leq D_{synth}\}/1000. \tag{7}$$

A larger ratio p also indicates that the data follow a power law with the estimated scaling parameter. A word of caution has to be made, though. It has been shown in *Clauset et al.* [2009] that a decreasing number of observations automatically increases the ratio p. And in Table 2 we are varying the upper cutoff point, such that one might suspect that this is the reason for the increasing p value (it remains an open question how to determine reliably the upper cutoff point s_{max}). However, as one can see the number of observations for the intervals between [8, 150] and [8, 120] stays almost constant at roughly $m \approx 1500$. Finally, we also mention that if one does not estimate the lower bound but determines a τ-m.l.e in the range of [2, 1200], one obtains $\hat{\tau} \approx 1.1292$. We thus conclude that the estimated $\hat{\tau}$ values lie in the range of 1.09 to 1.12 with high confidence, see Figure 4. Consequently, the estimated τ is ≈ 1.1 and dramatically lower than previously suggested, see above.

4. Conclusion

The task of estimating the power law exponent associated with a residual cluster size distribution is both intriguing and important.

One aim of this paper was to illustrate very clearly that the method from *Dias and Wilkinson* [1986] based on (4) as an approximation of (3) is strongly biased and will not generate a consistent τ estimate as it simply defines τ to be larger than 2—irrespective of the underlying data.

The maximum likelihood method [*Clauset et al.*, 2009], however, is mathematically rigorous; the m.l.e. of τ is consistent. We therefore conclude that the high p value of 94.4% for the interval [8, 120], see Table 2, indicates that for this common data set $\tau \approx 1.1$.

Thus, in summary, we conclude that the scaling exponent of a typical residual cluster size distribution is significantly smaller than previously suggested [*Iglauer et al.*, 2011, 2010, 2013, 2012; *Georgiadis et al.*, 2013; *Andrew et al.*, 2014], particularly by the *summation methods* from *Dias and Wilkinson* [1986]. This raises increasing doubt that simple percolation models can predict multiphase flow through rock with high accuracy (note that percolation theory predicts $\tau = 2.189$ [*Larson et al.*, 1977; *Stauffer*, 1979; *Lorenz and Ziff*, 1998]). Furthermore, $\tau \approx 1.1$ implies that oil recovery is easier than previously assumed, while CO_2 geostorage is more risky.

Acknowledgments
The authors would like to thank three anonymous referees for very valuable comments. And both authors are particularly indebted to Lukas for his continuing support during the preparation of this paper.

References

Al-Yaseri, A. Z., M. Lebedev, S. J. Vogt, M. L. Johns, A. Barifcani, and S. Iglauer (2015), Pore-scale analysis of formation damage in Bentheimer sandstone with in-situ NMR and micro-computed tomography experiments, *J. Pet. Sci. Eng.*, *129*(21), 48–57, doi:10.1016/j.petrol.2015.01.018.

Andrew, M., B. Bijeljic, and M. J. Blunt (2014), Pore-scale imaging of trapped supercritical carbon dioxide in sandstones and carbonates, *Int. J. Greenhouse Gas Control*, *22*, 1–14, doi:10.1016/j.ijggc.2013.12.018.

Buades, A., B. Coll, and J. M. Morel (2005), A non-local algorithm for image denoising, *Proc. CVPR IEEE*, *2*, 60–65.

Chatzis, I., N. R. Morrow, and H. T. Lim (1983), Magnitude and detailed structure of residual oil saturation, *SPE J.*, *23*, 311–326.

Chaudhary, K., M. Bayani Cardenas, W. W. Wolfe, J. A. Maisano, R. A. Ketcham, and P. C. Bennett (2013), Pore-scale trapping of supercritical CO_2 and the role of grain wettability and shape, *Geophys. Res. Lett.*, *40*, 3878–3882, doi:10.1002/grl.50658.

Clauset, A., C. R. Shalizi, and M. E. J. Newman (2009), Power-law distributions in empirical data, *SIAM Rev.*, *51*, 661–703.

Dias, M. M., and D. Wilkinson (1986), Percolation with trapping, *J. Phys. A Math. Gen.*, *19*, 3131–3146.

Geistlinger, H., and S. Mohammadian (2015), Capillary trapping mechanism in strongly water wet systems: Comparison between experiment and percolation theory, *Adv. Water Resour.*, *79*, 35–50.

Georgiadis, A., S. Berg, A. Makurat, G. Maitland, and H. Ott (2013), Pore-scale micro-computed tomography imaging: Nonwetting-phase cluster-size distribution during drainage and imbibition, *Phys. Rev. E*, *88*, 033002.

Herring, A. L., E. J. Harper, L. Andersson, A. Sheppard, B. K. Bay, and D. Wildenschild (2013), Effect of fluid topology on residual nonwetting phase trapping: Implications for geologic CO_2 sequestration, *Adv. Water Resour.*, *62*, 47–58.

Iglauer, S., S. Favretto, G. Spinelli, G. Schena, and M. J. Blunt (2010), X-ray tomography measurements of power-law cluster size distributions for the nonwetting phase in sandstones, *Phys. Rev. E*, *82*, 056315, doi:10.1103/PhysRevE.82.056315.

Iglauer, S., A. Paluszny, C. H. Pentland, and M. J. Blunt (2011), Residual CO_2 imaged with X-ray micro-tomography, *Geophys. Res. Lett.*, *38*, L21403, doi:10.1029/2011GL049680.

Iglauer, S., M. A. Fernø, P. Shearing, and M. J. Blunt (2012), Comparison of residual oil cluster size distribution, morphology and saturation in oil-wet and water-wet sandstone, *J. Colloid Interface Sci.*, *375*, 187–192.

Iglauer, S., A. Paluszny, and M. J. Blunt (2013), Simultaneous oil recovery and residual gas storage: a pore-level analysis using in situ X-ray micro-tomography, *Fuel*, *103*, 905–914.

Iglauer, S., C. Geng, M. Sarmadivaleh, and M. Lebedev (2014), A pore scale analysis of a surfactant flooding procedure using in-situ X-ray micro-computed tomography, paper presented at International Petroleum Conference, Doha, 20–24 Jan.

Karpyn, Z., M. Piri, and G. Singh (2010), Experimental investigation of trapped oil clusters in a water-wet bead pack using X-ray microtomography, *Water Resour. Res.*, *46*, W04510, doi:10.1029/2008WR007539.

Kumar, M., T. Senden, M. Knackstedt, S. Latham, W. Pinczewski, R. Sok, and A. Sheppard (2009), Sheppard A, Turner M imaging of pore scale distribution of fluids and wettability, *Petrophysics*, *50*, 311–321.

Kumar, M., A. Fogden, T. Senden, and M. Knackstedt (2012), Investigation of pore-scale mixed wettability, *SPE J.*, *17*, 20–30.

Lake, L. W. (2010), *Enhanced Oil Recovery*, SPE, Richardson, Tex.

Larson, R. G., L. E. Scriven, and H. T. Davis (1977), Percolation theory of residual phases in porous media, *Nature*, *268*, 409–413, doi:10.1038/268409a0.

Lindgren, B. W. (1993), *Statistical Theory*, 4th ed., Chapman and Hall, London and New York.

Lorenz, C. D., and R. M. Ziff (1998), Precise determination of the bond percolation thresholds and finite-size scaling corrections for the sc, fcc and bcc lattices, *Phys. Rev. E*, *57*, 230–236.

Maloney, D. R., M. M. Honarpour, and A. D. Brinkmeyer (1990), The effects of rock characteristics on relative permeability. Topical Report, National Institute for Petroleum and Energy Research, Bartlesville, Oklahoma, *Eur. J. Neurosci.*, *28*, 1654–1660.

Pentland, C. H., R. El-Maghraby, S. Iglauer, and M. J. Blunt (2011), Measurements of the capillary trapping of super-critical carbon dioxide in Berea sandstone, *Geophys. Res. Lett.*, *38*, L06401, doi:10.1029/2011GL046683.

Pentland, C. H., S. Iglauer, O. Gharbi, K. Okada, and T. Suekane (2012), The influence of pore space geometry on the entrapment of carbon dioxide by capillary forces, paper SPE 158516 presented at SPE Asia Pacific Oil and Gas Conference and Exhibition, Perth, Aust., 22–24 Oct.

Prodanovic, M., W. B. Lindquist, and R. S. Seright (2007), 3D image-based characterization of fluid displacement in a Berea core, *Adv. Water Resour.*, *30*, 214–226.

Riaz, A., M. Hesse, H. A. Tchelepi, and F. M. Orr (2006), Onset of convection in a gravitationally unstable diffusive boundary layer in porous media, *J. Fluid Mech.*, *548*, 87–111.

Schlüter, S., A. Sheppard, K. Brown, and D. Wildenschild (2014), Image processing of multiphase images obtained via X-ray microtomography: A review, *Water Resour. Res.*, *50*, 3615–3639, doi:10.1002/2014WR015256.

Sleep, B. E., and P. D. McClure (2001), Removal of volatile and semivolatile organic contamination from soil by air and steam flushing, *J. Contam. Hydrol.*, *50*, 21–40.

Stauffer, D. (1979), Scaling theory of percolation clusters, *Phys. Rep.*, *54*, 1–74.

Suekane, T., T. Nobuso, S. Hirai, and M. Kiyota (2008), Geological storage of carbon dioxide by residual gas and solubility trapping, *Int. J. Greenhouse Gas Control*, *2*(1), 58–64, doi:10.1016/S1750-5836(07)00096-5.

Wardlaw, N. C., and Y. Li (1988), Fluid topology, pore size and aspect ratio during imbition., *Transp. Porous Media*, *3*, 17–34.

Yang, Z., I. Neuweiler, Y. Méheust, F. Fagerlund, and A. Niemi (2015), Fluid trapping during capillary displacement in fractures, *Adv. Water Resour.*, *95*, 264, doi:10.1016/j.advwatres.2015.07.015.